

# Nanoscale Advances

Accepted Manuscript

This article can be cited before page numbers have been issued, to do this please use: H. Chen, A. Udepurkar, C. Clasen, V. Sebastian and S. Kuhn, *Nanoscale Adv.*, 2026, DOI: 10.1039/D5NA00897B.



This is an Accepted Manuscript, which has been through the Royal Society of Chemistry peer review process and has been accepted for publication.

Accepted Manuscripts are published online shortly after acceptance, before technical editing, formatting and proof reading. Using this free service, authors can make their results available to the community, in citable form, before we publish the edited article. We will replace this Accepted Manuscript with the edited and formatted Advance Article as soon as it is available.

You can find more information about Accepted Manuscripts in the [Information for Authors](#).

Please note that technical editing may introduce minor changes to the text and/or graphics, which may alter content. The journal's standard [Terms & Conditions](#) and the [Ethical guidelines](#) still apply. In no event shall the Royal Society of Chemistry be held responsible for any errors or omissions in this Accepted Manuscript or any consequences arising from the use of any information it contains.

# Enabling Porous Nanospheres with Highly Efficient Drug Loading and Sustained Release through a Thermal-Controlled Continuous Stirred-Tank Reactor Cascade

Huiyu Chen<sup>a, †</sup>, Aniket Pradip Udepurkar<sup>a,b, †</sup>, Christian Clasen<sup>c</sup>, Victor Sebastián Cabeza<sup>d,e,f,g</sup>, Simon Kuhn<sup>a\*</sup>

<sup>a</sup> Department of Chemical Engineering, Process Engineering for Sustainable Systems (ProcESS), KU Leuven, Celestijnenlaan 200F, Leuven 3001, Belgium

<sup>b</sup> Department of Chemical Engineering, Massachusetts Institute of Technology, 77 Massachusetts Avenue, Cambridge, MA 02139, USA

<sup>c</sup> Department of Chemical Engineering, Soft Matter, Rheology and Technology (SMaRT), KU Leuven, Celestijnenlaan 200J, Leuven 3001, Belgium

<sup>d</sup> Instituto de Nanociencia y Materiales de Aragón (INMA), CSIC-Universidad de Zaragoza, Zaragoza 50009, Spain

<sup>e</sup> Department of Chemical and Environmental Engineering Universidad de Zaragoza Campus Rio Ebro, 50018 Zaragoza, Spain

<sup>f</sup> Laboratorio de Microscopías Avanzadas, Universidad de Zaragoza, 50018 Zaragoza, Spain

<sup>g</sup> Networking Research Center on Bioengineering, Biomaterials and Nanomedicine (CIBER-BBN), 28029 Madrid, Spain

\* Corresponding author. E-mail address: [simon.kuhn@kuleuven.be](mailto:simon.kuhn@kuleuven.be) (S. Kuhn)

† These authors contributed equally to this work.

**ABSTRACT:**

Nanospheres hold great promise for drug delivery but face challenges in achieving both high drug loading and sustained release. Here, we present a novel approach to produce porous cyclosporin A-loaded poly(lactic-co-glycolic acid) (PLGA) nanospheres via a thermal-controlled continuous stirred-tank reactor (CSTR) cascade, featuring rapid solidification of nanoemulsion droplets. This process traps more drug molecules in the nanosphere core by limiting their diffusion towards the surface and surrounding medium, resulting in a core-loaded structure. The resulting PLGA nanospheres exhibit a high cyclosporin A loading capacity and enable sustained drug release through the hydrolytic degradation of the PLGA matrix. Moreover, the total synthesis time is reduced from several hours to 40 min. The CSTR assisted manufacturing approach offers an efficient route for engineering nanospheres with high drug payloads and improved release kinetics, with broad potential for nanomedicine manufacturing.

**KEYWORDS:** poly(lactic-co-glycolic acid) nanospheres, continuous stirred-tank reactor cascade, drug loading, sustained drug release, porous nanospheres



Open Access Article. Published on 23 December 2025. Downloaded on 12/24/2025 2:49:02 PM.  
This article is licensed under a Creative Commons Attribution 3.0 Unported Licence.



Nanoscale Advances Accepted Manuscript

**INTRODUCTION**

Drug-loaded nanospheres represent a powerful strategy for delivering active pharmaceutical ingredients using inert nanoscale carriers. These nanospheres can protect drug molecules from degradation and promote their transport across biological barriers to reach a target site<sup>1–4</sup>. The inert materials, such as biodegradable polymers, enable sustained drug release, thus allowing for tailored pharmacokinetic properties and reduce the need for repeated dosing<sup>5,6</sup>. Moreover, increasing the drug load per nanosphere allows higher doses per injection, improving patient compliance and minimizing excipient-related side effects<sup>7–9</sup>. For many treatments, achieving a high therapeutic mass fraction is a prerequisite due to strict volume limits on injectable formulations (0.1 mL intradermal, 1 mL subcutaneous, and 1–3 mL intramuscular)<sup>10</sup>. These constraints make the development of nanospheres with high drug content critically important.

Engineering high drug-loaded nanospheres is challenging due to inherent limitations arising from their high surface-to-volume ratio. Drugs positioned on the particle surface are susceptible to loss during the formulation and post-formulation processes<sup>11–13</sup>. Nanospheres are primarily composed of non-therapeutic scaffold polymers, such as poly(lactic-co-glycolic acid) (PLGA). Drug loadings in most reported studies are lower than 4%, some are even substantially below 1%<sup>11,14–27</sup>. Various strategies have been developed to improve drug loading efficiency through strengthening drug-carrier interactions, such as donor-receptor coordination and covalent conjugation<sup>28–31</sup>. However, these approaches are limited, as they require both the drug and carrier molecules to have specific structural and chemical properties.

Encapsulating a larger fraction of drug molecules within the nanosphere core, rather than leaving a significant portion on the surface, helps to overcome surface-to-volume ratio constraints and enhances overall drug loading. This strategy eliminates the dependence on specific molecular

features of the drug and carrier. A core-loaded nanosphere structure not only increases the total drug content but also offers better control over the drug release. Drug release from nanospheres occurs in two phases: an initial burst release caused by the rapid diffusion of surface-located drugs, followed by a more sustained release through the hydrolytic degradation of the PLGA matrix<sup>32–34</sup>. By increasing the amount of drug loaded in the core, the initial burst release and resulting toxicity risks can be reduced, leading to a more sustained and prolonged release profile. The nanospheres could be formed from nanoemulsion droplets as the organic solvent evaporates (**Figure 1c**), leading us to reasonably hypothesize that the solvent removal process would play a critical role in determining the solidification of drug and polymer molecules. By optimizing this process, it may be possible to fabricate core-loaded nanospheres with high drug loading and improved release kinetics.

For continuous nanosphere synthesis, microfluidic nanoprecipitation is used in many studies<sup>6,35–38</sup>. Although this technique can produce ultra-small nanospheres ranging from 20 to 100 nm, it struggles with a low drug loading capacity ( $< 4\%$ )<sup>14,39–41</sup>. Increasing the particle size can improve drug loading, but it will compromise the ability to cross biological barriers. This hinders in particular applications like brain-targeted delivery, which requires particles to be below 100 nm to cross the blood-brain barrier<sup>42–44</sup>. Furthermore, the small channel sizes required for rapid mixing in microfluidics can lead to issues like low throughput and microchannel clogging<sup>45–47</sup>.

Another commonly used synthesis method is emulsion-solvent evaporation. In 2007, Budhian et al.<sup>20</sup> attempted to increase drug loading by adjusting the pH during solvent evaporation to reduce drug diffusion into the aqueous phase. However, they achieved a maximum drug loading of 2.5%. In 2016, de Solorzano et al.<sup>48</sup> used microchannel emulsification for high-throughput synthesis ( $\sim 10$  g/h) of Cyclosporin A-loaded PLGA nanospheres. However, the resulting particles had a



mean size far exceeding 200 nm. Recently, Operti et al.<sup>49</sup> introduced an inline sonicator for continuous emulsification, but the solvent evaporation was performed in a batch mode with dilution and stirring for 1 hour, and the smallest mean particle size achieved was 184.7 nm. To conclude, the synthesis of drug-loaded PLGA nanospheres through emulsion-solvent evaporation has not been fully transitioned to a continuous process. Achieving a mean particle size under 100 nm remains challenging, and the impact of solvent evaporation temperature on drug encapsulation has been largely overlooked in previous studies.

In this work, we control the solvent removal process using a continuous stirred-tank reactor (CSTR) cascade (**Figure 1b**), which provides thermal regulation, to solidify the drug and polymer molecules. This approach contrasts with previous studies<sup>48–51</sup>, where solvent removal was performed in batch mode and remained largely unoptimized. This continuous manufacturing strategy eliminates batch-to-batch variations and provides a well-defined scale-up pathway<sup>52,53</sup>, addressing two major challenges in the industrialization of nanomedicines<sup>54–58</sup>. To validate our approach, cyclosporin A (CyA) is selected as a model peptide drug due to its poor water solubility and limited bioavailability (class II from the Biopharmaceutical Classification System, BCS). The solvent removal step is systematically optimized, and its impact on particle size distribution, morphology, and drug loading efficiency of cyclosporin A-loaded PLGA nanospheres (CyA-PLGA NPs) is assessed. Furthermore, *in vitro* drug release studies are conducted to evaluate the sustained release profile. Process efficiency and residual solvent content are also analysed to ensure the robustness and scalability of the developed method.



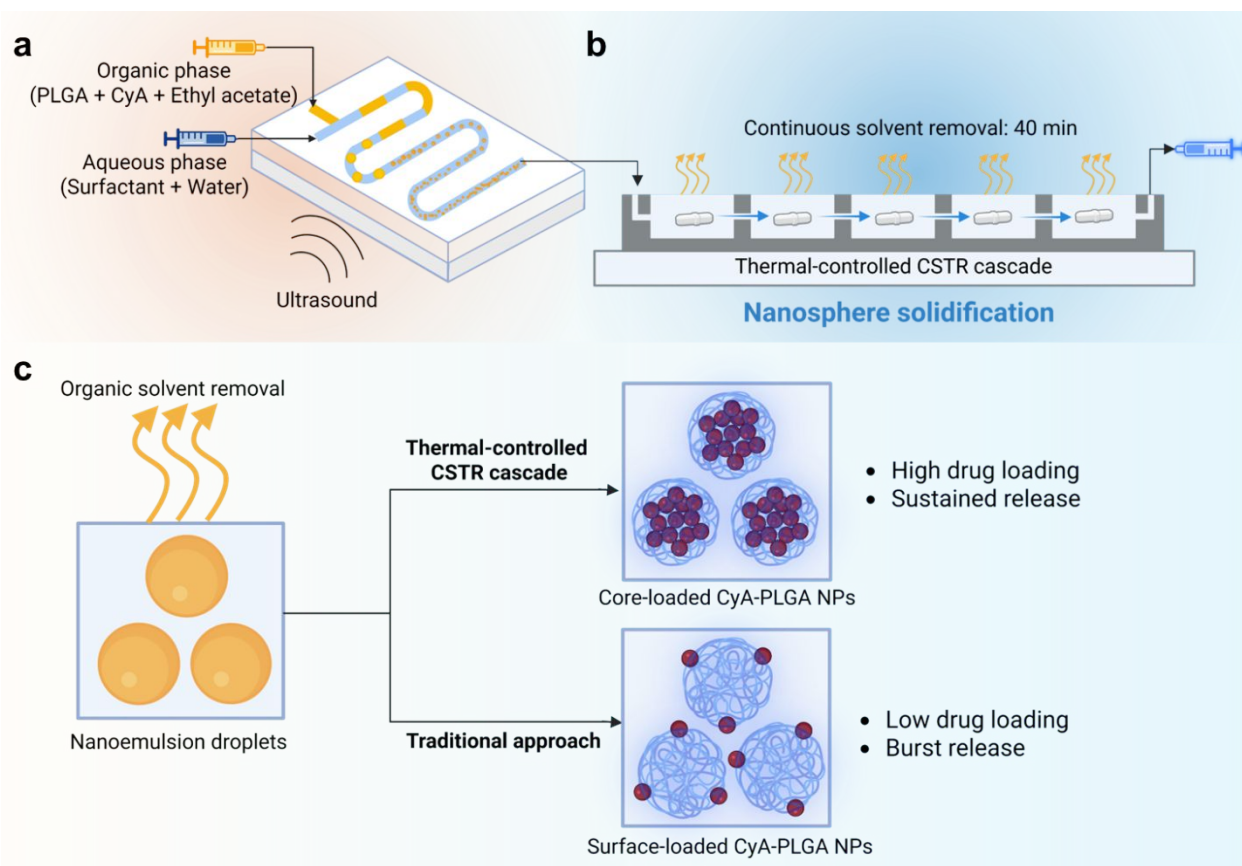


**Figure 1.** Synthesis process of cyclosporin A-loaded PLGA nanospheres (CyA-PLGA NPs). The setup consists of (a) an ultrasonic microreactor for emulsion generation and (b) a continuous thermal-controlled CSTR cascade for solvent removal and nanosphere solidification. (c) Solvent removal and solidification processes at the droplet/particle level, along with the resulting nanosphere properties, compared to the traditional batch approach. Illustration created with BioRender.com.

## RESULTS AND DISCUSSION

### Synthesis and characterization of CyA-PLGA NPs

CyA-PLGA NPs were synthesized using the emulsion–solvent evaporation technique. In the first step, an automated ultrasonic microreactor was employed to generate nanoemulsion droplets. The





119 organic phase, consisting of PLGA and cyclosporin A dissolved in ethyl acetate, and the aqueous  
120 phase, consisting of the surfactant Poloxamer 407 in Milli-Q water, were introduced into the  
121 microreactor. Ultrasonic energy was applied via a piezoelectric transducer plate attached to the  
122 bottom of the reactor to facilitate emulsification (**Figure 1a**). Following droplet formation, the  
123 nanoemulsion was fed into a CSTR cascade for continuous thermal-controlled solvent removal  
124 (**Figure 1b**). The outlet of the CSTR cascade was connected to a syringe pump, which  
125 continuously withdrew the solidified CyA-PLGA NP suspension. The temperature of the CSTR  
126 cascade was regulated by a circulating water jacket located beneath the wells (**Figure 3a**). The  
127 entire process was automated and conducted at a constant flow rate of 250  $\mu\text{L}/\text{min}$ , with an overall  
128 residence time of  $\sim 40$  min. For comparison, a traditional batch method was carried out by  
129 collecting the nanoemulsion from the microreactor outlet into a glass vial (**Figure 3b**), followed  
130 by magnetic stirring for at least 4 hours at room temperature to allow for solvent evaporation.

131 For effective drug delivery, nanospheres smaller than 200 nm with a polydispersity index (PDI)  
132 below 0.2 are desired<sup>59,60</sup>, while brain-targeted therapies typically demand even smaller sizes—  
133 under 100 nm<sup>42,44,61</sup>. To meet these criteria, the emulsification step in the ultrasonic microreactor  
134 was systematically optimized (**Table S2**) before integrating the thermal-controlled CSTR cascade.

135 After implementing the CSTR cascade for continuous solvent removal, the process temperature  
136 was varied from room temperature ( $\sim 23$  °C) to 45 °C. Across this temperature range, the resulting  
137 CyA-PLGA NPs consistently maintained a mean particle size below 82 nm and a PDI below 0.2,  
138 fulfilling the size distribution requirements for biomedical applications. The pore size distribution  
139 results from the Brunauer–Emmett–Teller (BET) analysis (**Figure 2d**) indicate the presence of  
140 micropores around 1.5 nm and mesopores in the 2–3 nm range. Larger pores ( $>5$  nm) are likely  
141 due to interstitial voids between the nanospheres. The coexistence of micropores and mesopores





is further confirmed by the t-plot curve, which exhibits a characteristic profile typical of micro-mesoporous materials<sup>62</sup>. SEM and TEM images revealed a smooth, spherical morphology with a uniform size distribution. No significant morphological differences were observed between nanoparticles synthesized at ~23 °C (**Figure S10**) and at 35 °C (**Figure 2e–f**), indicating that the mild thermal treatment does not compromise particle integrity. Additionally, the CyA-PLGA NPs demonstrated good storage stability, retaining their size distribution for at least 30 days when stored at 2–8 °C (**Figure 2g**).

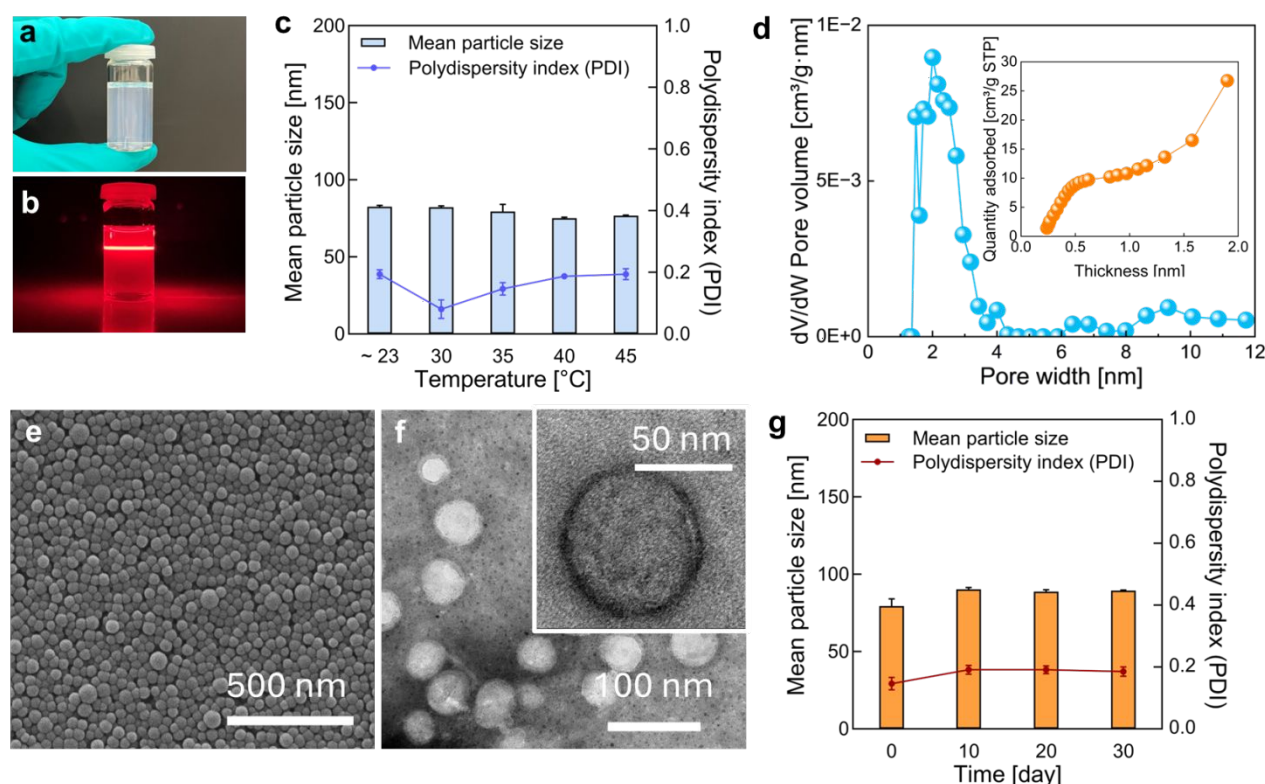


**Figure 2.** Characterizations of CyA-PLGA NPs. (a) Visual appearance of the CyA-PLGA NP suspension. (b) Tyndall effect observed in the suspension using a laser pointer. (c) Mean particle size and polydispersity index (PDI) measured by dynamic light scattering (DLS). (d) Porosity distribution determined by Density Functional Theory (DFT) analysis and t-plot analysis of CyA-



PLGA NPs based on Brunauer-Emmett-Teller (BET) isotherms, measured at standard temperature and pressure (STP, 273 K and 101.325 kPa) with N<sub>2</sub>. Representative (e) scanning electron microscopy (SEM) image, (f) Transmission electron microscopy (TEM) images, and (g) stability profile over 30 days (storage 2-8°C) of CyA-PLGA NPs prepared via the thermal-controlled CSTR cascade at 35 °C. Data are presented as mean ± SD (n = 3).

**Thermal-controlled CSTR cascade for enhanced drug loading**

The solvent removal time was significantly reduced from over 4 hours<sup>63</sup> to just 40 min by replacing the conventional batch method (**Figure 3b**) with a continuous CSTR cascade (**Figure 3a**), which doubled the surface-to-volume ratio (**Table S1**). At a fixed duration of 40 min and room temperature (~23 °C), the residual ethyl acetate concentration decreased from 141.3 µL/mL (batch) to 8.0 µL/mL (CSTR), demonstrating the improved efficiency. However, to meet EMA regulations for Class 3 solvents<sup>64</sup>, which require residual levels below 5 µL/mL (5000 ppm), faster solvent removal is necessary. This was addressed by introducing thermal control at elevated temperatures.

The residual ethyl acetate content in each CSTR well during solvent removal (**Figure 3c**) and in the final nanosphere suspension (**Figure 3d**), along with the drug loading (DL, **Figure 3e**) and encapsulation efficiency (EE, **Figure 3f**) of the resulting CyA-PLGA NPs, were quantified by HPLC. Results showed that at 30°C and 35°C the final residual ethyl acetate was significantly reduced to 2.3 ± 0.3 µL/mL and 0.9 ± 0.3 µL/mL, respectively, both well below the 5 µL/mL threshold. Interestingly, a slight increase in residual solvent was observed at 40 °C (1.5 ± 0.4 µL/mL) and 45 °C (2.4 ± 0.1 µL/mL). The drug loading increased from 4.2 ± 1.3% at ~23 °C to a peak value of 7.6 ± 0.4% at 35 °C, but then declined to 3.6 ± 0.7% and 3.9 ± 0.3% at 40 °C and 45 °C, respectively, even below the value at room temperature (~23°C). A similar trend was

observed for the encapsulation efficiency, which rose from  $26.5 \pm 8.5\%$  to  $49.0 \pm 2.5\%$  at  $35^\circ\text{C}$ , and then decreased to  $22.7 \pm 4.6\%$  and  $24.4 \pm 2.2\%$  at the higher temperatures.

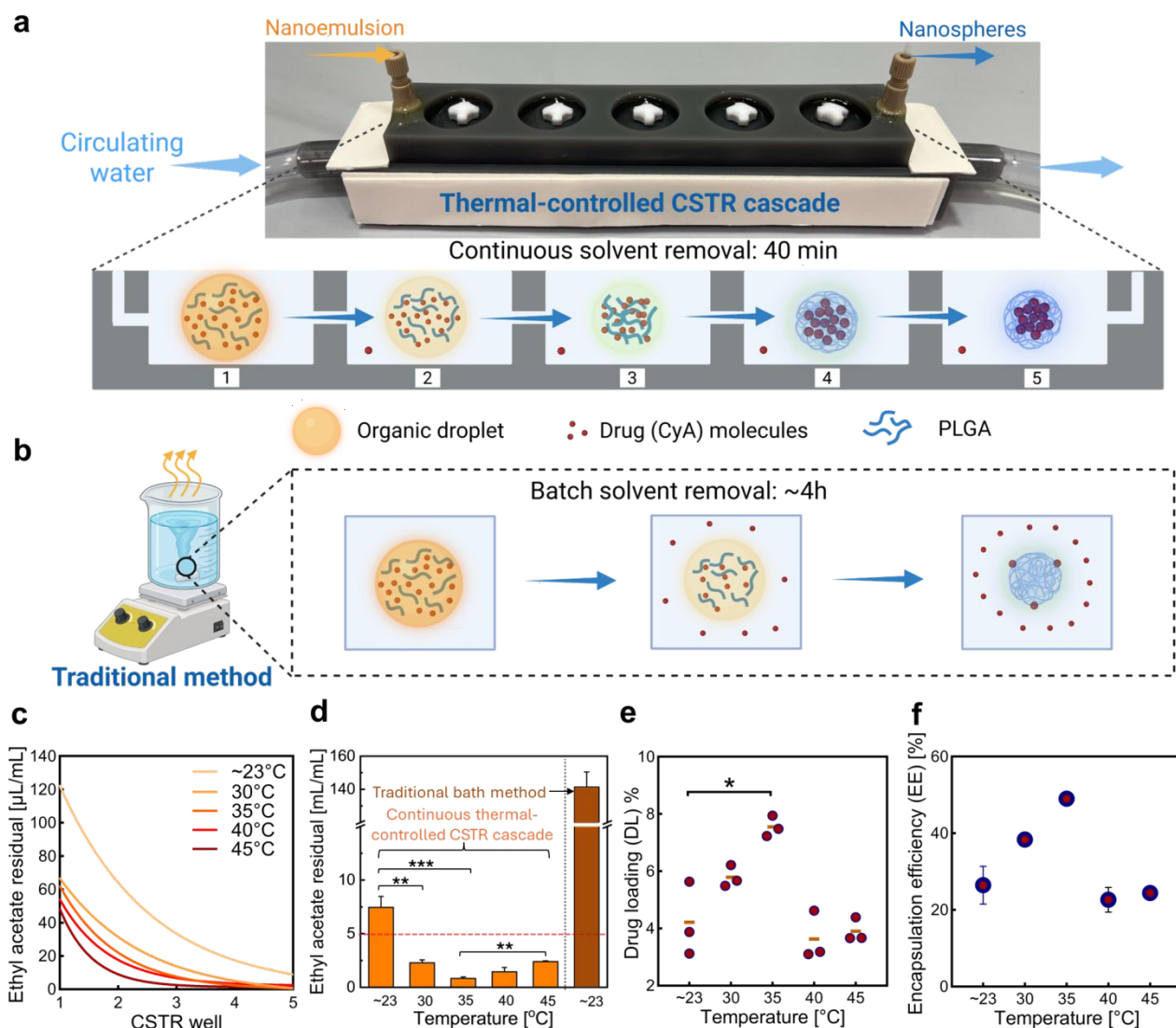


**Figure 3.** Optimization of the thermal-controlled CSTR cascade and the resulting enhancement in drug loading efficiency. Schematic comparison of the organic solvent removal and nanoparticle formation process using (a) thermal-controlled CSTR cascade and (b) traditional batch method. (c) Residual ethyl acetate concentrations measured in each CSTR well (1–5) during the solvent removal process. (d) Final residual solvent content in the nanoparticle suspension. (e) Drug



loading (DL) and (f) encapsulation efficiency (EE) of the resulting CyA-PLGA NPs obtained at varying CSTR cascade temperatures (~23°C to 45°C). In graphic (d), the red dashed line indicates the maximum allowed residual level of ethyl acetate according to EMA guidelines (5 µL/mL). Data are shown as mean ± SD, n = 3. Statistical significance is indicated as \*p < 0.05, \*\*p < 0.01, \*\*\*p < 0.001. Only relevant and significant statistical comparisons are highlighted.

The initial reduction in residual ethyl acetate at moderately elevated temperatures is attributed to an accelerated solvent removal rate, as further supported by measurements from individual CSTR wells (1-5) during the process (**Figure 3c**). The observed improvement in drug loading efficiency results from more efficient solvent removal achieved through thermal-controlled CSTR cascade. During this process, the organic solvent must first diffuse from the emulsion droplets into the surrounding aqueous phase before it can evaporate<sup>65,66</sup>. Katou et al.<sup>67</sup> proposed a mathematical model to describe the kinetics of this solvent transfer from oil droplets to the aqueous phase:

$$\frac{\partial C_d}{\partial t} = \frac{D}{r^2} \cdot \frac{\partial}{\partial r} \cdot \left( r^2 \cdot \frac{\partial C_d}{\partial r} \right) \quad (1)$$

where  $C_d$  stands for solvent concentration,  $t$  for time,  $r$  for radial position, and  $D$  for the solvent diffusion coefficient. According to the Wilke–Chang equation, the solvent diffusion coefficient  $D$  is given by:

$$D = \frac{7.4 * 10^{-8} (\phi M)^{1/2} T}{\eta V^{0.6}} \quad (2)$$

where  $\phi$  is the association parameter,  $M$  the molecular mass of the solvent,  $T$  the temperature,  $\eta$  the viscosity, and  $V$  the molecular volume. The diffusion coefficient is proportional to the temperature, meaning that at higher temperatures, solvent removal occurs more rapidly. This accelerates droplet solidification and limits the time available for drug diffusion into the external



aqueous phase. As a result, a larger amount of the drug is retained within the polymeric matrix of the nanospheres, significantly enhancing drug loading.

However, at further elevated temperatures of 40 °C and 45 °C—surpassing the glass transition temperature ( $T'_g$ ) of PLGA (**Figure S11**)—the polymer does not solidify into a rigid, glassy state but instead transitions into a softer, rubbery phase<sup>68–70</sup>. In this rubbery state, stronger polymer–solvent interactions hinder solvent diffusion and evaporation, resulting in higher residual ethyl acetate levels despite the elevated temperature. Moreover, this rubbery state leads to two major effects: i) the diffusion of the organic solvent slows down considerably, giving the drug more time to diffuse out of the polymeric matrix and escape into the aqueous phase, reducing drug retention; ii) in some cases, the polymer-drug mixture fails to solidify into nanoparticles before reaching the liquid surface during evaporation. Instead, it forms a polymeric film on the liquid surface in the CSTR (as observed during experiments), leading to a loss of drug material and reduced nanoparticle formation. Consequently, the drug loading efficiency at 40 °C and 45 °C declined, even falling below that achieved at room temperature (~23 °C).

Therefore, 35°C was determined to be the optimal solvent removal temperature in the CSTR cascade, as it enables ideal particle size distribution, maximizes the drug loading efficiency, and minimizes the residual ethyl acetate content, while preventing the detrimental effects of PLGA transitioning into its rubbery state above  $T'_g$ .

To confirm that these improvements were due to the nature of the thermal-controlled CSTR cascade nanotechnology, rather than temperature alone, a batch solvent removal was also performed at 35 °C for comparison (**Table S4**). When the batch process was run for the same duration as the CSTR cascade (40 min), the drug loading efficiency was extremely low at



0.8 ± 0.1%, indicating that almost no drug was encapsulated. As previously discussed, this is attributed to the poor solvent removal efficiency of the batch method, which left a high residual ethyl acetate concentration (91.9 ± 1.6 µL/mL). With the aqueous phase nearing saturation, the diffusion of ethyl acetate from the droplets was restricted, significantly slowing solidification. This prolonged diffusion window allowed drug molecules to escape into the aqueous phase before being entrapped. Even after extending the batch evaporation to 4 hours, the drug loading efficiency only modestly increased to 2.5 ± 0.9%, still far below the value achieved with the CSTR cascade. These results confirm that the significant improvement in drug loading was primarily due to the efficient solvent removal enabled by the thermal-controlled CSTR cascade.

### *In vitro* drug release

The release of a poorly water-soluble drug from PLGA nanospheres typically happens in two phases (**Figure 4a**). The first phase is a rapid initial burst release, driven by the diffusion of the drug located near the particle surface. The second phase is more sustained and is attributed to the hydrolysis of the PLGA and erosion of the polymeric matrix, which releases the drug encapsulated in the nanosphere core<sup>32–34</sup>. If the enhanced solvent removal rate indeed results in increased drug encapsulation in the nanosphere core, CyA-PLGA NPs synthesized using the thermal-controlled CSTR cascade at 35°C should exhibit less of an initial burst release and more drug release during the second sustained phase.





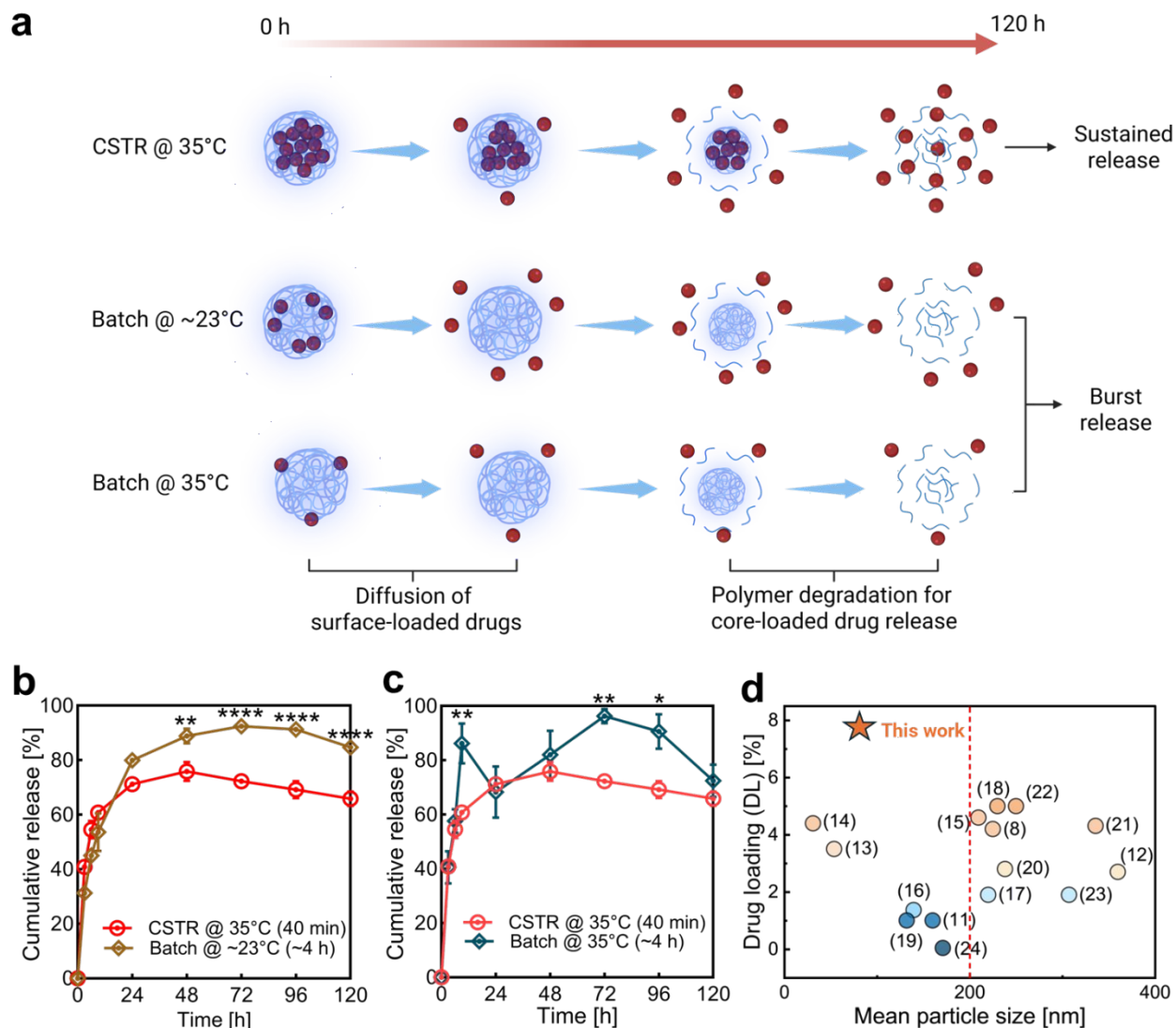


**Figure 4.** *In vitro* drug release demonstrating the advantage of core-loaded nanoparticle structure. (a) Schematic illustration of the two-phase drug release mechanism from PLGA nanoparticles. Sustained and burst release profiles resulting from core-loaded and surface-loaded drug distributions, respectively. (b–c) *In vitro* drug release data of CyA-PLGA NPs prepared via the thermal-controlled CSTR cascade at 35 °C (CSTR @ 35 °C), compared to those prepared using the traditional batch method at room temperature (Batch @ ~23 °C) and at 35 °C (Batch @ 35 °C). Data are presented as mean  $\pm$  SD ( $n = 3$ ). Statistical significance is indicated as follows:





253  $*P < 0.05$ ;  $**P < 0.01$ ;  $***P < 0.001$ ;  $****P < 0.0001$ . (d) Positioning our core-loaded CyA-  
254 PLGA NPs within the landscape of benchmark studies<sup>11,14–27</sup>, highlighting their exceptional ability  
255 to simultaneously achieve both a high drug loading efficiency and a small particle size (two critical  
256 and often mutually exclusive parameters in nanoparticle synthesis). The red dashed line in panel  
257 (d) marks the  $<200$  nm threshold typically considered suitable for drug delivery applications.

258 To provide a meaningful comparison, we selected the batch solvent evaporation at  $\sim 23^{\circ}\text{C}$  (Batch  
259 @  $\sim 23^{\circ}\text{C}$ ) to represent the slowest evaporation rate. The drug release profile over 120 h, depicted  
260 in **Figure 4b**, confirms the hypothesis. During the first 24 hours of the initial release phase, there  
261 was no statistically significant difference between the two samples. However, by the end of the  
262 burst release phase (72 h), 93% of the drug encapsulated in the Batch @  $\sim 23^{\circ}\text{C}$  nanospheres was  
263 released, indicating that a major fraction of the CyA molecules was located close to the surface. In  
264 contrast, the CSTR @  $35^{\circ}\text{C}$  nanospheres only released 76% of their drug content during the initial  
265 burst phase (48 h), leaving 24% encapsulated within the nanosphere core for a slower, sustained  
266 release. The cumulative drug release gradually declined in the second phase, as the drug continued  
267 to be released, but at a slower rate than its degradation, making the net change appear negative.  
268 This trend aligns with the CyA stability profile observed in our degradation test (**Figure S9**) and  
269 is consistent with findings reported in other studies<sup>71,72</sup>.

270 Next, we conducted an additional *in vitro* drug release study on CyA-PLGA NPs prepared via  
271 batch solvent evaporation at  $35^{\circ}\text{C}$  (Batch @  $35^{\circ}\text{C}$ ). The aim was to assess whether the core-  
272 loaded drug distribution observed in nanospheres produced by the CSTR cascade resulted  
273 primarily from the high solvent removal efficiency of the thermal-controlled CSTR cascade  
274 process, or if similar characteristics could be achieved by applying the same elevated temperature  
275 in a conventional batch process. As shown in **Figure 4c**, the Batch @  $35^{\circ}\text{C}$  nanospheres exhibited



276 a sharp burst release, with 86% of the encapsulated drug released within the very first 9 h. This  
277 release was even more abrupt than that of the Batch @  $\sim 23^\circ\text{C}$  nanospheres, suggesting that the  
278 drug was located even closer to the particle surface. By 24 hours, the CyA concentration in the  
279 release medium had already begun to decline due to degradation, and the drop was more  
280 pronounced because there was little to no sustained release between 9 and 24 hours to replenish  
281 the drug. In the end, the sustained release phase began after 48 h, corresponding to the release of  
282 the remaining 14% of the drug from the nanosphere core.

283 Based on the drug release results, we can conclude that the Batch @  $35^\circ\text{C}$  nanospheres contained  
284 a larger fraction of drug encapsulated in the core (14%) compared to the Batch @  $\sim 23^\circ\text{C}$   
285 nanospheres (7%), but still less than the CSTR @  $35^\circ\text{C}$  nanospheres (24%). This suggests that the  
286 elevated temperature did enhance solvent diffusion from the droplets into the aqueous phase,  
287 allowing more drug to be retained in the nanoparticle core. However, the batch process is limited  
288 by a low surface-to-volume ratio, making the evaporation of solvent from the aqueous phase into  
289 air the rate-limiting step. This inefficiency resulted in a high residual solvent concentration in the  
290 aqueous phase, which in turn suppressed further diffusion of organic solvent from the droplets.  
291 Consequently, solvent accumulated at the droplet/nanoparticle interface, providing more time for  
292 drug molecules to diffuse into the aqueous phase and be lost, leading to the lower drug loading  
293 efficiency ( $2.5 \pm 0.9\%$ ) compared to the CSTR @  $35^\circ\text{C}$  ( $7.6 \pm 0.4\%$ ). Moreover, this solvent  
294 accumulation forces a larger portion of the drug toward the sphere surface, as evidenced by a rapid  
295 burst release of 86% of the drug within the first 9 h, in contrast to the slower burst release observed  
296 in Batch @  $\sim 23^\circ\text{C}$  nanospheres (93% released over 48 h). Therefore, the improvement was not  
297 solely due to the elevated temperature, but was primarily driven by the high solvent removal  
298 efficiency achieved through the thermal-controlled CSTR cascade.



## CONCLUSIONS

In summary, we have developed a thermal-controlled CSTR cascade nanotechnology for the synthesis of CyA-PLGA NPs, achieving a significantly improved drug loading efficiency and a more sustained release profile. The formation of nanospheres with high drug loading is a result of a larger fraction of drug molecules solidifying at the particle core, realized by a more efficient solvent removal in the CSTR cascade at 35°C. The achieved drug loading is, to our knowledge, the highest reported for sub-100 nm CyA-PLGA NPs, significantly exceeding the previously reported maximum of 4.6%<sup>11,14–27</sup> (**Figure 4d**). The core-loaded structure not only provides a higher drug payload, but also enables gradual release of drug molecules. The sustained release from high drug-loaded nanospheres may contribute to an enhanced therapeutic efficacy and reduced adverse effects for drug delivery applications. Additionally, the robustness and scalability of the thermal-controlled CSTR cascade provide a promising pathway for clinical translation, aligning with FDA guidelines for modern pharmaceutical manufacturing<sup>73</sup>.

## Author Contributions

H.C. and A.P.U. contributed equally to this work. Conceptualization: H.C., A.P.U. and V.S.C. Methodology: H.C., A.P.U. and V.S.C. Experiment: H.C., A.P.U., and V.S.C. Writing—original draft: H.C. and A.P.U. Writing—review and editing: C.C., V.S.C., and S.K. Data curation: H.C. and A.P.U. Supervision: C.C., V.S.C., and S.K. Funding acquisition: S.K.

## Conflicts of interest

There are no conflicts to declare.

## Data availability



Data are available at <http://xxx>. The Supplementary Information (SI) includes materials and methods, supplementary results on nanosphere synthesis, imaging, degradation studies, and numerical data corresponding to the plotted figures.

## Acknowledgements

Financial support from the Research Foundation Flanders (G0B5921N, G088922N) is acknowledged. V.S.C. acknowledges support from the Spanish Ministry of Science and Innovation (grant PID2021-127847OB-I00), as well as the NextGenerationEU/PRTR project (PDC2022-133866-I00), CIBER-BBN, ELECOMI and NANBIOSIS ICTSs. H.C. acknowledges FWO Flanders for a strategic basic PhD fellowship (1S06425N). The authors also thank Lisa De Vriendt and Elena Brozzi for their assistance with the DSC measurements; Keiran Mc Carogher and Lorian De Vrieze for their support in constructing the experimental setup; Prof. Erin Koos and Yanshen Zhu for providing access to and guidance with the DLS measurements; and Pieter Adriaenssens for his help with the HPLC analysis.

## REFERENCES

- (1) Blanco, E.; Shen, H.; Ferrari, M. Principles of Nanoparticle Design for Overcoming Biological Barriers to Drug Delivery. *Nature Biotechnology*. Nature Publishing Group September 8, 2015, pp 941–951. <https://doi.org/10.1038/nbt.3330>.
- (2) Chiang, M. R.; Hsu, C. W.; Pan, W. C.; Tran, N. T.; Lee, Y. S.; Chiang, W. H.; Liu, Y. C.; Chen, Y. W.; Chiou, S. H.; Hu, S. H. Reprogramming Dysfunctional Dendritic Cells by a Versatile Catalytic Dual Oxide Antigen-Captured Nanosponge for Remotely Enhancing Lung Metastasis Immunotherapy. *ACS Nano* 2025, 19 (2), 2117–2135. <https://doi.org/10.1021/acsnano.4c09525>.
- (3) Huynh, T. M. H.; Huang, P. X.; Wang, K. L.; Tran, N. T.; Iao, H. M.; Pan, W. C.; Chang, Y. H.; Lien, H. W.; Lee, A. Y. L.; Chou, T. C.; Chiang, W. H.; Hu, S. H. Reprogramming Immunodeficiency in Lung Metastases via PD-L1 siRNA Delivery and Antigen Capture of Nanosponge-Mediated Dendritic Cell Modulation. *ACS Nano* 2025, 19 (27), 25134–25153. <https://doi.org/10.1021/acsnano.5c05395>.
- (4) Yalamandala, B. N.; Chen, Y. J.; Lin, Y. H.; Huynh, T. M. H.; Chiang, W. H.; Chou, T. C.; Liu, H. W.; Huang, C. C.; Lu, Y. J.; Chiang, C. S.; Chu, L. A.; Hu, S. H. A Self-Cascade Penetrating Brain Tumor Immunotherapy Mediated by Near-Infrared II Cell Membrane-



- 349 Disrupting Nanoflakes via Detained Dendritic Cells. *ACS Nano* 2024, 18 (28), 18712–18728.  
350 <https://doi.org/10.1021/acsnano.4c06183>.
- 351 (5) Brigham, N. C.; Ji, R. R.; Becker, M. L. Degradable Polymeric Vehicles for Postoperative Pain  
352 Management. *Nature Communications*. *Nature Research* December 1, 2021.  
353 <https://doi.org/10.1038/s41467-021-21438-3>.
- 354 (6) Liu, D.; Zhang, H.; Fontana, F.; Hirvonen, J. T.; Santos, H. A. Microfluidic-Assisted  
355 Fabrication of Carriers for Controlled Drug Delivery. *Lab on a Chip*. Royal Society of Chemistry  
356 June 7, 2017, pp 1856–1883. <https://doi.org/10.1039/c7lc00242d>.
- 357 (7) Shen, S.; Wu, Y.; Liu, Y.; Wu, D. High Drug-Loading Nanomedicines: Progress, Current  
358 Status, and Prospects. *International Journal of Nanomedicine*. Dove Medical Press Ltd. May 31,  
359 2017, pp 4085–4109. <https://doi.org/10.2147/IJN.S132780>.
- 360 (8) Della Rocca, J.; Liu, D.; Lin, W. Are High Drug Loading Nanoparticles the next Step Forward  
361 for Chemotherapy? *Nanomedicine*. March 2012, pp 303–305. <https://doi.org/10.2217/nnm.11.191>.
- 362 (9) Chen, W.; Zhou, S.; Ge, L.; Wu, W.; Jiang, X. Translatable High Drug Loading Drug Delivery  
363 Systems Based on Biocompatible Polymer Nanocarriers. *Biomacromolecules*. American Chemical  
364 Society June 11, 2018, pp 1732–1745. <https://doi.org/10.1021/acs.biomac.8b00218>.
- 365 (10) Sienkiewicz S.; Palmunen J. *Clinical Nursing Calculations*. Jones & Bartlett Learning 2015.
- 366 (11) Govender, T.; Stolnik, S.; Garnett, M. C.; Illum, L.; Davis, S. S. PLGA Nanoparticles  
367 Prepared by Nanoprecipitation: Drug Loading and Release Studies of a Water Soluble Drug. *J.*  
368 *Controlled Release* 1999, 57 (2), 171–185. [https://doi.org/10.1016/S0168-3659\(98\)00116-3](https://doi.org/10.1016/S0168-3659(98)00116-3).
- 369 (12) Chin, S. F.; Jimmy, F. B.; Pang, S. C. Size Controlled Fabrication of Cellulose Nanoparticles  
370 for Drug Delivery Applications. *J Drug Deliv Sci Technol* 2018, 43, 262–266.  
371 <https://doi.org/10.1016/j.jddst.2017.10.021>.
- 372 (13) Rodrigues de Azevedo, C.; von Stosch, M.; Costa, M. S.; Ramos, A. M.; Cardoso, M. M.;  
373 Danhier, F.; Préat, V.; Oliveira, R. Modeling of the Burst Release from PLGA Micro- and  
374 Nanoparticles as Function of Physicochemical Parameters and Formulation Characteristics. *Int J*  
375 *Pharm* 2017, 532 (1), 229–240. <https://doi.org/10.1016/J.IJPHARM.2017.08.118>.
- 376 (14) Todaro, B.; Moscardini, A.; Luin, S. Pioglitazone-Loaded PLGA Nanoparticles: Towards the  
377 Most Reliable Synthesis Method. *Int J Mol Sci* 2022, 23 (5).  
378 <https://doi.org/10.3390/ijms23052522>.
- 379 (15) Cheng, J.; Teply, B. A.; Sherifi, I.; Sung, J.; Luther, G.; Gu, F. X.; Levy-Nissenbaum, E.;  
380 Radovic-Moreno, A. F.; Langer, R.; Farokhzad, O. C. Formulation of Functionalized PLGA-PEG  
381 Nanoparticles for in Vivo Targeted Drug Delivery. *Biomaterials* 2007, 28 (5), 869–876.  
382 <https://doi.org/10.1016/j.biomaterials.2006.09.047>.
- 383 (16) Cheow, W. S.; Hadinoto, K. Factors Affecting Drug Encapsulation and Stability of Lipid-  
384 Polymer Hybrid Nanoparticles. *Colloids Surf B Biointerfaces* 2011, 85 (2), 214–220.  
385 <https://doi.org/10.1016/j.colsurfb.2011.02.033>.
- 386 (17) Zhang, C. X.; Cheng, Y.; Liu, D. Z.; Liu, M.; Cui, H.; Zhang, B. Le; Mei, Q. B.; Zhou, S. Y.  
387 Mitochondria-Targeted Cyclosporin A Delivery System to Treat Myocardial Ischemia  
388 Reperfusion Injury of Rats. *J Nanobiotechnology* 2019, 17 (1). <https://doi.org/10.1186/s12951-019-0451-9>.
- 389 (18) Takeuchi, I.; Kagawa, A.; Makino, K. Skin Permeability and Transdermal Delivery Route of  
390 30-Nm Cyclosporin A-Loaded Nanoparticles Using PLGA-PEG-PLGA Triblock Copolymer.  
391 *Colloids Surf A Physicochem Eng Asp* 2020, 600, 124866.  
392 <https://doi.org/10.1016/J.COLSURFA.2020.124866>.





- (19) Song, X.; Zhao, Y.; Hou, S.; Xu, F.; Zhao, R.; He, J.; Cai, Z.; Li, Y.; Chen, Q. Dual Agents Loaded PLGA Nanoparticles: Systematic Study of Particle Size and Drug Entrapment Efficiency. *European Journal of Pharmaceutics and Biopharmaceutics* 2008, 69 (2), 445–453. <https://doi.org/10.1016/J.EJPB.2008.01.013>.
- (20) Budhian, A.; Siegel, S. J.; Winey, K. I. Haloperidol-Loaded PLGA Nanoparticles: Systematic Study of Particle Size and Drug Content. *Int J Pharm* 2007, 336 (2), 367–375. <https://doi.org/10.1016/J.IJPHARM.2006.11.061>.
- (21) Betancourt, T.; Brown, B.; Brannon-Peppas, L. Doxorubicin-Loaded PLGA Nanoparticles by Nanoprecipitation: Preparation, Characterization and In Vitro Evaluation. *Nanomedicine* 2007, 2 (2), 219–232. <https://doi.org/10.2217/17435889.2.2.219>.
- (22) Fonseca, C.; Simões, S.; Gaspar, R. Paclitaxel-Loaded PLGA Nanoparticles: Preparation, Physicochemical Characterization and in Vitro Anti-Tumoral Activity. *Journal of Controlled Release* 2002, 83 (2), 273–286. [https://doi.org/10.1016/S0168-3659\(02\)00212-2](https://doi.org/10.1016/S0168-3659(02)00212-2).
- (23) Dillen, K.; Vandervoort, J.; Van Den Mooter, G.; Verheyden, L.; Ludwig, A. Factorial Design, Physicochemical Characterisation and Activity of Ciprofloxacin-PLGA Nanoparticles. *Int J Pharm* 2004, 275 (1–2), 171–187. <https://doi.org/10.1016/J.IJPHARM.2004.01.033>.
- (24) R.S., P.; Bomb, K.; Srivastava, R.; Bandyopadhyaya, R. Dual Drug Delivery of Curcumin and Niclosamide Using PLGA Nanoparticles for Improved Therapeutic Effect on Breast Cancer Cells. *Journal of Polymer Research* 2020, 27 (5), 133. <https://doi.org/10.1007/s10965-020-02092-7>.
- (25) Albisa, A.; Piacentini, E.; Sebastian, V.; Arruebo, M.; Santamaria, J.; Giorno, L. Preparation of Drug-Loaded PLGA-PEG Nanoparticles by Membrane-Assisted Nanoprecipitation. *Pharm Res* 2017, 34 (6), 1296–1308. <https://doi.org/10.1007/s11095-017-2146-y>.
- (26) Anwer, K.; Mohammad, M.; Ezzeldin, E.; Fatima, F.; Alalaiwe, A.; Iqbal, M. Preparation of Sustained Release Apremilast-Loaded PLGA Nanoparticles: In Vitro Characterization and in Vivo Pharmacokinetic Study in Rats. *Int J Nanomedicine* 2019, Volume 14, 1587–1595. <https://doi.org/10.2147/IJN.S195048>.
- (27) Manchanda, R.; Fernandez-Fernandez, A.; Nagesetti, A.; McGoron, A. J. Preparation and Characterization of a Polymeric (PLGA) Nanoparticulate Drug Delivery System with Simultaneous Incorporation of Chemotherapeutic and Thermo-Optical Agents. *Colloids Surf B Biointerfaces* 2010, 75 (1), 260–267. <https://doi.org/10.1016/J.COLSURFB.2009.08.043>.
- (28) Lv, S.; Wu, Y.; Cai, K.; He, H.; Li, Y.; Lan, M.; Chen, X.; Cheng, J.; Yin, L. High Drug Loading and Sub-Quantitative Loading Efficiency of Polymeric Micelles Driven by Donor-Receptor Coordination Interactions. *J Am Chem Soc* 2018, 140 (4), 1235–1238. <https://doi.org/10.1021/jacs.7b12776>.
- (29) Shen, Y.; Jin, E.; Zhang, B.; Murphy, C. J.; Sui, M.; Zhao, J.; Wang, J.; Tang, J.; Fan, M.; Van Kirk, E.; Murdoch, W. J. Prodrugs Forming High Drug Loading Multifunctional Nanocapsules for Intracellular Cancer Drug Delivery. *J Am Chem Soc* 2010, 132 (12), 4259–4265. <https://doi.org/10.1021/ja909475m>.
- (30) Cai, K.; He, X.; Song, Z.; Yin, Q.; Zhang, Y.; Uckun, F. M.; Jiang, C.; Cheng, J. Dimeric Drug Polymeric Nanoparticles with Exceptionally High Drug Loading and Quantitative Loading Efficiency. *J Am Chem Soc* 2015, 137 (10), 3458–3461. <https://doi.org/10.1021/ja513034e>.
- (31) Li, D.; Tang, G.; Yao, H.; Zhu, Y.; Shi, C.; Fu, Q.; Yang, F.; Wang, X. Formulation of PH-Responsive PEGylated Nanoparticles with High Drug Loading Capacity and Programmable Drug Release for Enhanced Antibacterial Activity. *Bioact Mater* 2022, 16, 47–56. <https://doi.org/10.1016/J.BIOACTMAT.2022.02.018>.



- 440 (32) Sánchez, A.; Vila-Jato, L.; Alonso, M. J. Development of biodegradable microspheres and  
441 nanospheres for the controlled release of cyclosporin A. *Int. J. Pharm.* 1993, 99, 263–273.  
442 [https://doi.org/10.1016/0378-5173\(93\)90369-Q](https://doi.org/10.1016/0378-5173(93)90369-Q)
- 443 (33) Yee Win, S.; Chavalitsarot, M.; Eawsakul, K.; Ongtanasup, T.; Nasongkla, N. Encapsulation  
444 of Cyclosporine A-Loaded PLGA Nanospheres in Alginate Microbeads for Anti-Inflammatory  
445 Application. *ACS Omega* 2024, 9 (6), 6901–6911. <https://doi.org/10.1021/acsomega.3c08438>.
- 446 (34) Fredenberg, S.; Wahlgren, M.; Reslow, M.; Axelsson, A. The Mechanisms of Drug Release  
447 in Poly(Lactic-Co-Glycolic Acid)-Based Drug Delivery Systems—A Review. *Int J Pharm* 2011,  
448 415 (1–2), 34–52. <https://doi.org/10.1016/J.IJPHARM.2011.05.049>.
- 449 (35) Min, K. I.; Im, D. J.; Lee, H. J.; Kim, D. P. Three-Dimensional Flash Flow Microreactor for  
450 Scale-up Production of Monodisperse PEG-PLGA Nanoparticles. *Lab Chip* 2014, 14 (20), 3987–  
451 3992. <https://doi.org/10.1039/c4lc00700j>.
- 452 (36) Wang, J.; Chen, W.; Sun, J.; Liu, C.; Yin, Q.; Zhang, L.; Xianyu, Y.; Shi, X.; Hu, G.; Jiang,  
453 X. A Microfluidic Tubing Method and Its Application for Controlled Synthesis of Polymeric  
454 Nanoparticles. *Lab Chip* 2014, 14 (10), 1673–1677. <https://doi.org/10.1039/c4lc00080c>.
- 455 (37) Le, P. T.; An, S. H.; Jeong, H. H. Microfluidic Tesla Mixer with 3D Obstructions to  
456 Exceptionally Improve the Curcumin Encapsulation of PLGA Nanoparticles. *Chemical*  
457 *Engineering Journal* 2024, 483, 149377. <https://doi.org/10.1016/J.CEJ.2024.149377>.
- 458 (38) Liu, Z.; Yang, M.; Zhao, Q.; Yao, C.; Chen, G. Scale-up of Antisolvent Precipitation Process  
459 with Ultrasonic Microreactors: Cavitation Patterns, Mixing Characteristics and Application in  
460 Nanoparticle Manufacturing. *Chemical Engineering Journal* 2023, 475, 146040.  
461 <https://doi.org/10.1016/J.CEJ.2023.146040>.
- 462 (39) Li, W.; Chen, Q.; Baby, T.; Jin, S.; Liu, Y.; Yang, G.; Zhao, C. X. Insight into Drug  
463 Encapsulation in Polymeric Nanoparticles Using Microfluidic Nanoprecipitation. *Chem Eng Sci*  
464 2021, 235, 116468. <https://doi.org/10.1016/J.CES.2021.116468>.
- 465 (40) Bai, X.; Tang, S.; Butterworth, S.; Tirella, A. Design of PLGA Nanoparticles for Sustained  
466 Release of Hydroxyl-FK866 by Microfluidics. *Biomaterials Advances* 2023, 154, 213649.  
467 <https://doi.org/10.1016/J.BIOADV.2023.213649>.
- 468 (41) Rocas, C. B.; Christensen, D.; Perrie, Y. Translating the Fabrication of Protein-Loaded  
469 Poly(Lactic-Co-Glycolic Acid) Nanoparticles from Bench to Scale-Independent Production Using  
470 Microfluidics. *Drug Deliv Transl Res* 2020, 10 (3), 582–593. <https://doi.org/10.1007/s13346-019-00699-y>.
- 471 (42) Wohlfart, S.; Gelperina, S.; Kreuter, J. Transport of Drugs across the Blood–Brain Barrier by  
472 Nanoparticles. *Journal of Controlled Release* 2012, 161 (2), 264–273.  
473 <https://doi.org/10.1016/J.JCONREL.2011.08.017>.
- 474 (43) Liu, D.; Lin, B.; Shao, W.; Zhu, Z.; Ji, T.; Yang, C. In Vitro and in Vivo Studies on the  
475 Transport of PEGylated Silica Nanoparticles across the Blood-Brain Barrier. *ACS Appl Mater*  
476 *Interfaces* 2014, 6 (3), 2131–2136. <https://doi.org/10.1021/am405219u>.
- 477 (44) Betzer, O.; Shilo, M.; Opoichinsky, R.; Barnoy, E.; Motiei, M.; Okun, E.; Yadid, G.;  
478 Popovtzer, R. The Effect of Nanoparticle Size on the Ability to Cross the Blood-Brain Barrier: An  
479 in Vivo Study. *Nanomedicine* 2017, 12 (13), 1533–1546. <https://doi.org/10.2217/nnm-2017-0022>.
- 480 (45) Tahir, N.; Madni, A.; Li, W.; Correia, A.; Khan, M. M.; Rahim, M. A.; Santos, H. A.  
481 Microfluidic Fabrication and Characterization of Sorafenib-Loaded Lipid-Polymer Hybrid  
482 Nanoparticles for Controlled Drug Delivery. *Int J Pharm* 2020, 581.  
483 <https://doi.org/10.1016/j.ijpharm.2020.119275>.





- (46) Leung, M. H. M.; Shen, A. Q. Microfluidic Assisted Nanoprecipitation of PLGA Nanoparticles for Curcumin Delivery to Leukemia Jurkat Cells. *Langmuir* 2018, 34 (13), 3961–3970. <https://doi.org/10.1021/acs.langmuir.7b04335>.
- (47) Rezvantlab, S.; Keshavarz Moraveji, M. Microfluidic Assisted Synthesis of PLGA Drug Delivery Systems. *RSC Advances*. Royal Society of Chemistry 2019, pp 2055–2072. <https://doi.org/10.1039/C8RA08972H>.
- (48) De Solorzano, I. O.; Uson, L.; Larrea, A.; Miana, M.; Sebastian, V.; Arruebo, M. Continuous Synthesis of Drug-Loaded Nanoparticles Using Microchannel Emulsification and Numerical Modeling: Effect of Passive Mixing. *Int J Nanomedicine* 2016, 11, 3397–3416. <https://doi.org/10.2147/IJN.S108812>.
- (49) Operti, M. C.; Bernhardt, A.; Sincari, V.; Jager, E.; Grimm, S.; Engel, A.; Hruby, M.; Figdor, C. G.; Tagit, O. Industrial Scale Manufacturing and Downstream Processing of PLGA-Based Nanomedicines Suitable for Fully Continuous Operation. *Pharmaceutics* 2022, 14 (2). <https://doi.org/10.3390/pharmaceutics14020276>.
- (50) Mainardes, R. M.; Evangelista, R. C. PLGA Nanoparticles Containing Praziquantel: Effect of Formulation Variables on Size Distribution. *Int J Pharm* 2005, 290 (1–2), 137–144. <https://doi.org/10.1016/J.IJPHARM.2004.11.027>.
- (51) Jaiswal, J.; Gupta, S. K.; Kreuter, J. Preparation of Biodegradable Cyclosporine Nanoparticles by High-Pressure Emulsification-Solvent Evaporation Process. *Journal of Controlled Release* 2004, 96 (1), 169–178. <https://doi.org/10.1016/J.JCONREL.2004.01.017>.
- (52) Cherkasov, N.; Adams, S. J.; Bainbridge, E. G. A.; Thornton, J. A. M. Continuous Stirred Tank Reactors in Fine Chemical Synthesis for Efficient Mixing, Solids-Handling, and Rapid Scale-Up. *Reaction Chemistry and Engineering*. Royal Society of Chemistry October 26, 2022, pp 266–277. <https://doi.org/10.1039/d2re00232a>.
- (53) Nandiwale, K. Y.; Hart, T.; Zahrt, A. F.; Nambiar, A. M. K.; Mahesh, P. T.; Mo, Y.; Nieves-Remacha, M. J.; Johnson, M. D.; García-Losada, P.; Mateos, C.; Rincón, J. A.; Jensen, K. F. Continuous Stirred-Tank Reactor Cascade Platform for Self-Optimization of Reactions Involving Solids. *React Chem Eng* 2022. <https://doi.org/10.1039/d2re00054g>.
- (54) Chan, H. W.; Chow, S.; Zhang, X.; Kwok, P. C. L.; Chow, S. F. Role of Particle Size in Translational Research of Nanomedicines for Successful Drug Delivery: Discrepancies and Inadequacies. *J Pharm Sci* 2023, 112 (9), 2371–2384. <https://doi.org/10.1016/J.XPHS.2023.07.002>.
- (55) Operti, M. C.; Bernhardt, A.; Grimm, S.; Engel, A.; Figdor, C. G.; Tagit, O. PLGA-Based Nanomedicines Manufacturing: Technologies Overview and Challenges in Industrial Scale-Up. *Int J Pharm* 2021, 605. <https://doi.org/10.1016/j.ijpharm.2021.120807>.
- (56) Desai, N. Challenges in Development of Nanoparticle-Based Therapeutics. *AAPS Journal*. June 2012, pp 282–295. <https://doi.org/10.1208/s12248-012-9339-4>.
- (57) Metselaar, J. M.; Lammers, T. Challenges in Nanomedicine Clinical Translation. *Drug Deliv Transl Res* 2020, 10 (3), 721–725. <https://doi.org/10.1007/s13346-020-00740-5>.
- (58) Hua, S.; de Matos, M. B. C.; Metselaar, J. M.; Storm, G. Current Trends and Challenges in the Clinical Translation of Nanoparticulate Nanomedicines: Pathways for Translational Development and Commercialization. *Frontiers in Pharmacology*. Frontiers Media S.A. July 17, 2018. <https://doi.org/10.3389/fphar.2018.00790>.
- (59) Banik, B. L.; Fattahi, P.; Brown, J. L. Polymeric Nanoparticles: The Future of Nanomedicine. *Wiley Interdisciplinary Reviews: Nanomedicine and Nanobiotechnology*. Wiley-Blackwell March 1, 2016, pp 271–299. <https://doi.org/10.1002/wnan.1364>.



- 531 (60) Doane, T. L.; Burda, C. The Unique Role of Nanoparticles in Nanomedicine: Imaging, Drug  
532 Delivery and Therapy. *Chem Soc Rev* 2012, 41 (7), 2885. <https://doi.org/10.1039/c2cs15260f>.
- 533 (61) Zha, S.; Liu, H.; Li, H.; Li, H.; Wong, K.-L.; Homayoun All, A. Functionalized Nanomaterials  
534 Capable of Crossing the Blood–Brain Barrier. *ACS Nano* 2024, 18 (3), 1820–1845.  
535 <https://doi.org/10.1021/acsnano.3c10674>.
- 536 (62) Mintova, S.; Čejka, J. Micro/Mesoporous Composites. *Stud Surf Sci Catal* 2007, 168, 301–  
537 VI. [https://doi.org/10.1016/S0167-2991\(07\)80797-X](https://doi.org/10.1016/S0167-2991(07)80797-X).
- 538 (63) Udepurkar, A. P.; Mampaey, L.; Clasen, C.; Sebastián Cabeza, V.; Kuhn, S. Microfluidic  
539 Synthesis of PLGA Nanoparticles Enabled by an Ultrasonic Microreactor. *React Chem Eng* 2024.  
540 <https://doi.org/10.1039/d4re00107a>.
- 541 (64) ICH Guideline Q3C (R8) on Impurities: Guideline for Residual Solvents, European Medicines  
542 Agency, 2022, Pp. 1-51.
- 543 (65) Arshady, R. Preparation of biodegradable microspheres and microcapsules: 2. Polyactides  
544 and related polyesters. *J. Control. Release* 1991, 17, 1-21. [https://doi.org/10.1016/0168-](https://doi.org/10.1016/0168-3659(91)90126-X)  
545 [3659\(91\)90126-X](https://doi.org/10.1016/0168-3659(91)90126-X)
- 546 (66) Wang, J.; Schwendeman, S. P. Mechanisms of Solvent Evaporation Encapsulation Processes:  
547 Prediction of Solvent Evaporation Rate. 1999. <https://doi.org/10.1021/js980169z>.
- 548 (67) Katou, H.; Wandrey, A. J.; Gander, B. Kinetics of Solvent Extraction/Evaporation Process  
549 for PLGA Microparticle Fabrication. *Int J Pharm* 2008, 364 (1), 45–53.  
550 <https://doi.org/10.1016/J.IJPHARM.2008.08.015>.
- 551 (68) Liu, G.; McEnnis, K. Glass Transition Temperature of PLGA Particles and the Influence on  
552 Drug Delivery Applications. *Polymers*. MDPI March 1, 2022.  
553 <https://doi.org/10.3390/polym14050993>.
- 554 (69) Park, K.; Otte, A.; Sharifi, F.; Garner, J.; Skidmore, S.; Park, H.; Jhon, Y. K.; Qin, B.; Wang,  
555 Y. Potential Roles of the Glass Transition Temperature of PLGA Microparticles in Drug Release  
556 Kinetics. *Molecular Pharmaceutics*. American Chemical Society January 4, 2021, pp 18–32.  
557 <https://doi.org/10.1021/acs.molpharmaceut.0c01089>.
- 558 (70) Park, P. I. P.; Jonnalagadda, S. Predictors of Glass Transition in the Biodegradable Polylactide  
559 and Poly-Lactide-Co-Glycolide Polymers. *J Appl Polym Sci* 2006, 100 (3), 1983–1987.  
560 <https://doi.org/10.1002/app.22135>.
- 561 (71) A. Abouelmagd, S.; Sun, B.; C. Chang, A.; Jin Ku, Y.; Yeo, Y. Release Kinetics Study of  
562 Poorly Water-Soluble Drugs from Nanoparticles: Are We Doing It Right? *Mol Pharm* 2015, 12  
563 (3), 997–1003. <https://doi.org/10.1021/mp500817h>.
- 564 (72) Tang, L.; Azzi, J.; Kwon, M.; Mounayar, M.; Tong, R.; Yin, Q.; Moore, R.; Skartsis, N.; Fan,  
565 T. M.; Abdi, R.; Cheng, J. Immunosuppressive Activity of Size-Controlled PEG-PLGA  
566 Nanoparticles Containing Encapsulated Cyclosporine A. *J Transplant* 2012, 2012, 1–9.  
567 <https://doi.org/10.1155/2012/896141>.
- 568 (73) U.S. Food and Drug Administration, Advancement of Emerging Technology Applications for  
569 Pharmaceutical Innovation and Modernization Guidance for Industry, 2017.  
570 <http://www.fda.gov/Drugs/GuidanceComplianceRegulatoryInformation/Guidances/default.htm>.



Data are available at <http://xxx>. The Supplementary Information (SI) includes materials and methods, supplementary results on nanosphere synthesis, imaging, degradation studies, and numerical data corresponding to the plotted figures.

